Theory and Experiments of Angular Vertical Comb-Drive Actuators for Scanning Micromirrors

Dooyoung Hah, Pamela R. Patterson, *Member, IEEE*, Hung D. Nguyen, *Student Member, IEEE*, Hiroshi Toshiyoshi, *Member, IEEE*, and Ming C. Wu, *Fellow, IEEE*

Abstract—We report on the theory and experiments of scanning micromirrors with angular vertical comb-drive (AVC) actuators. Parametric analyses of rotational vertical comb-drive actuators using a hybrid model that combines two-dimensional finite-element solutions with analytic formulations are described. The model is applied to both AVC and staggered vertical comb-drive (SVC) actuators. Detailed design tradeoffs and conditions for pull-in-free operations are discussed. Our simulation results show that the fringe fields play an important role in the estimation of maximum continuous rotation angles, particularly for combs with thin fingers, and that the maximum scan angle of the AVC is up to 60% larger than that of the SVC. Experimentally, a large dc continuous scan angle of 28.8° (optical) has been achieved with a moderate voltage (65 V) for a 1-mm-diameter scanning micromirror with AVC actuators. Excellent agreement between the experimental data and the theoretical simulations has been obtained.

Index Terms—Angular vertical comb-drive (AVC) actuator, micromirror, silicon-on-insulator (SOI) microelectromechanical systems (MEMS), staggered vertical comb-drive (SVC) actuator.

NOMENCLATURE

C	Capacitance.
C_{unit}	Capacitance of a unit cell with a moving finger and a fixed finger.
H_{offset}	Initial vertical offset between a moving and a fixed fingers exceeding the finger thickness in staggered vertical comb drives (SVCs).
$H_{\text{max,offset}}$	Maximum allowable initial vertical offset while avoiding pull-in in SVC.
h	Vertical offset between a moving and a fixed fingers in a plane perpendicular to the longitudinal direction (y) of the fingers [see Fig. 3(a)].
PI	Pull-in investigation function.
V	Applied voltage.
θ	Rotation angle.
θ_C	Rotation angle where a tip of a moving finger starts to overlap a fixed finger in angular vertical comb drives (AVCs).
θ_{fo}	Geometric angle defined as finger thickness over finger offset length.
θ_i	Initial comb angle in an AVC.
θ_M	Maximum continuous rotation angle.
θ_{mc}	Rotation angle where C is maximum.
θ_{PI}	Rotation angle where pull-in occurs (or a pull-in angle).

I. INTRODUCTION

RECENTLY, there has been increasing interest in vertical comb-drive actuators for scanning micromirror applications due to their high force density and wide continuous scan range. Although a variety of designs and fabrication methods have been reported, most of them can be divided into two categories: SVCs [1]–[8] and AVCs [9]–[14]. Unlike a lateral comb-drive actuator, a vertical comb-drive actuator requires a vertical offset between the moving fingers (rotor) and the fixed fingers (stator) for out-of-plane rotation. In an SVC, the moving fingers are offset vertically from the fixed fingers. The SVC scanners have been fabricated using wafer bonding [1]–[3], integration of polysilicon and bulk micromachining [4], double-side alignment lithography on a silicon-on-insulator (SOI) wafer [5], multistep etching [6], [7], and surface micromachining [8] technologies. Since the misalignment between the moving and the fixed fingers can result in lateral instability during actuation, fabrication methods for self-aligned SVCs have been developed by a number of groups [3], [6], [7]. In the AVC, the moving fingers are fabricated in the same layer as the fixed fingers and then tilted upward by self-assembly. Since all the fingers are patterned in a single-step etching process, the fingers are inherently self-aligned. The authors have demonstrated a 1-mm-diameter single-crystal silicon (SCS) micromirror with a self-assembled AVC realized by reflow of photoresist [9], [10]. Xie *et al.* employed stress-induced curling in a multilayered metal–oxide hinge to assemble the AVC [11]. Kim *et al.* utilized plastic deformation to build the AVC [12]. Torsion bars were mechanically deformed while heated above the glass transition temperature, causing a permanent plastic deformation.

Fig. 1 shows scanning electron micrographs (SEMs) of a fabricated micromirror. The inset is an enlarged view of the AVC. All the features on the SOI, including the mirror, the AVC, and the torsion springs, were patterned in a single photolithographic and deep reactive ion etching (DRIE) step. After release, the wafer was placed in deionized water (DIW) at ∼104 °C to reflow the photoresist hinge. The hinge remained rigid during actuation. The detailed fabrication process can be found in [10],
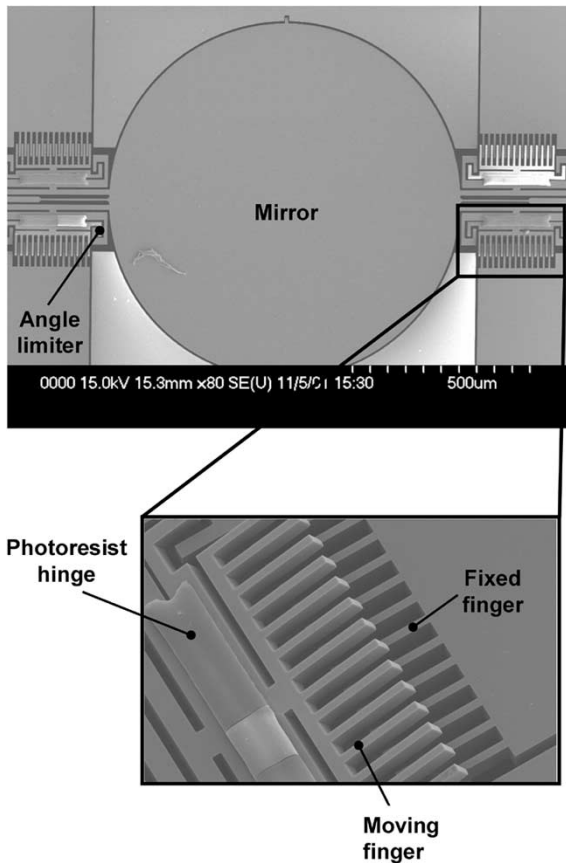
Fig. 1. SEM image of a scanning micromirror with angular vertical comb-drive actuators (enlarged view) assembled by reflow of photoresist hinge.

[17]. A resonant scan angle of $\pm 18°$ at 1.4 kHz has been obtained. The photoresist hinges were later replaced by benzocyclobutene (BCB) for better robustness and higher process yield [14], [17]. A surface- and bulk-micromachined AVC scanner with initial comb angle precisely defined by polysilicon structures has also been reported by our group [13]. DC scan angle of $\pm 4°$ (mechanical) at 40 V and a resonant frequency of 661 Hz were achieved.

In contrast to the common intuition that comb-drive actuators are always stable while parallel-plate actuators suffer from pull-in instability, both the AVC and the SVC could exhibit pull-in phenomena if not properly designed. Pull-in can be avoided by proper designs. Therefore, it is very important to establish an accurate and efficient model that is suitable for parametric analysis. Most of the models for rotational vertical comb drives reported to date employ parallel-plate approximation to estimate the overlap capacitance between the moving and the fixed comb fingers [4], [11]. The analytic model ignores the fringe field and, as we will demonstrate in this paper, often leads to inaccurate results, particularly for actuators with thin fingers. Though more accurate results can be obtained using commercial simulation tools with three-dimensional (3-D) finite-element analysis, they requires extensive computation time and are not suitable for parametric analysis. A hybrid model that combines 3-D capacitance extraction tool (FastCap) and polynomial fitting has been used to model translational vertical comb drives [15]. However, it is not suitable for

parametric analysis of rotational vertical comb drives, as each comb geometry/dimension requires a separate extraction of 3-D capacitance. Previously, we have developed a two-dimensional (2-D) hybrid model that combines analytical formulations with 2-D finite-element solutions to analyze a high fill-factor micromirror array with a hidden SVC [8]. Excellent agreement with the measured data has been obtained.

In this paper, we apply the hybrid model for parametric analysis of both the AVC and the SVC actuators. The conditions for pull-in-free operation are identified. The maximum continuous rotation angles (θ_M) of the AVC and the SVC are calculated using our hybrid 2-D model and compared with the simpler analytical models. Our results show that the maximum continuous rotation angles are underestimated in simple analytical models without considering fringe fields. We also show that the maximum scan angle of the AVC is up to 60% larger than that of the SVC for the same comb-finger dimensions. The simulation results of the AVC are compared with the experimental results, and excellent agreement has been achieved. The paper is organized as follows: first, the analytical models using parallel-plate approximations are derived for both AVCs and SVCs. Then the hybrid 2-D model is described in detail. Next, the maximum continuous rotation angles are calculated as a function of the angular (translational) offset between the moving and the fixed combs for the AVC (SVC). Parametric analyses are performed for the maximum scan angles of AVC and SVC. Finally, the calculated scanning characteristics of the AVC are compared with the experimental results.

II. ANALYSIS

In electrostatic actuators, the continuous actuation range is limited by either the maximum capacitance between moving and fixed electrodes or the pull-in phenomenon. When the capacitance of an actuator reaches its maximum value, it cannot move further because the force direction will be reversed. Pull-in occurs when the rate of increase of the electrostatic torque (or force) becomes larger than that of the mechanical restoring torque (or force), causing the moving electrodes to snap toward the fixed electrode. We have shown that for actuators with one degree of freedom, the pull-in condition is only related to the geometry of the electrodes and not dependent on spring structures [16]. The pull-in angle (or displacement) can be calculated as long as the angular (or positional) dependence of the capacitance (C) of the electrodes is known. It can be obtained by solving the following equation:

$$\text{PI}(\theta) = \frac{\partial C}{\partial \theta} - \theta \cdot \frac{\partial^2 C}{\partial \theta^2} = 0 \tag{1}$$

where $\text{PI}(\theta)$ is a *p*ull-in *i*nvestigation function and θ is rotation angle.

A. Simple Analytical Model

First, we describe the analytic models for both AVC and SVC. The schematic diagrams of the AVC and the SVC are depicted in Fig. 2. In the analytical model, the fringe capacitance is not taken into account and the vertical offset in SVC (H_{offset}) is set to zero. The capacitance (C_{AVC}) and the PI function (PI_{AVC})
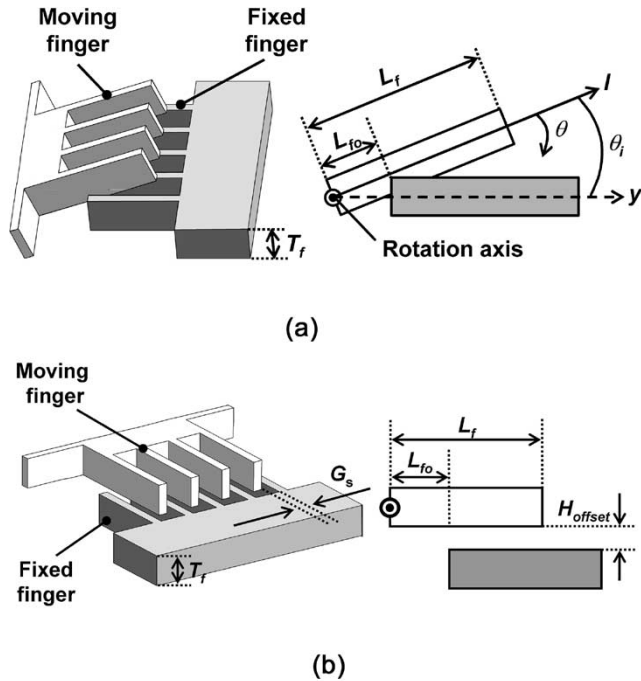
Fig. 2. Schematic diagrams of: (a) angular and (b) staggered vertical comb-drive actuators.

TABLE I
DIMENSIONS OF FABRICATED AVC

symbol	description	value
N_f	number of fingers	52
L_f	finger length	160 μm
D_{axis}	distance between assembly axis and actuation axis	50 μm
L_{fo}	finger offset length	71 μm
T_f	finger thickness	25 μm
W_f	finger width	4.9 μm
G_s	lateral finger spacing	3.1 μm
$T_s \times W_s \times L_s$	spring dimension	$25 \times 1.9 \times 200 \ \mu m^3$
θ_i	initial comb angle	12.4°

of the AVC can be expressed by (2a)–(3b) for small θ (which expressions are shown at the bottom of the page), where ϵ_0 is the permittivity of air, N_f is the number of comb fingers, T_f and L_f are the thickness and length of the fingers, respectively, L_{fo} is the offset between the tip of fixed fingers and the rotation axis, θ_i is the initial comb angle, and G_S is the lateral finger spacing. The notations are illustrated in Fig. 2 and summarized in Table I. Equation (3b) is always positive, implying there is no pull-in when the comb angle is between θ_i and θ_C defined in (2a). The pull-in angle, if it exists, must lie between zero and θ_C. By setting (3a) to zero, the pull-in angle of the AVC is found to be

$$\theta_{\mathrm{PI, \ AVC}} \cong \frac{\theta_i}{3} - \frac{8\theta_i^3}{81\theta_{\mathrm{fo}}^2 - 36\theta_i^2} = \frac{\theta_i}{3} - O\left(\theta_i, \theta_{\mathrm{fo}}\right) \quad (4)$$

where θ_{fo} is defined as T_f/L_{fo}. When θ_{fo} is sufficiently large compared to θ_i (i.e., $\theta_{\mathrm{fo}} \gg 0.86\theta_i$), the pull-in angle approaches to one-third of θ_i. There is no pull-in if the value of $\theta_{\mathrm{PI, \ AVC}}$ in

(4) is greater than θ_C; hence, the pull-in-free condition for AVC is

$$\frac{T_f}{L_f} \geq \frac{2}{3}\theta_i + O\left(\theta_i, \theta_{\mathrm{fo}}\right). \quad (5)$$

When there exists no pull-in, the maximum continuous rotation angle $(\theta_{M,\mathrm{AVC}})$ is determined by the angle $(\theta_{\mathrm{mc, \ AVC}})$ at which $C_{\mathrm{AVC}}(\theta)$ reaches maximum, which is exactly θ_i, and the maximum pull-in-free θ_i for a certain finger geometry is determined by (5). Therefore, $\theta_{M,\mathrm{AVC}}$ can be approximated by

$$\theta_{M,\mathrm{AVC}} \cong 1.5\frac{T_f}{L_f}. \quad (6)$$

The capacitance (C_{SVC}) and PI function $(\mathrm{PI}_{\mathrm{SVC}})$ of SVC can be simplified to the following expressions for small θ:

$$C_{\mathrm{SVC}}(\theta) = \frac{\varepsilon_0 N_f}{G_s}\left(L_f^2 - L_{\mathrm{fo}}^2\right)\theta \quad (7)$$

$$\mathrm{PI}_{\mathrm{SVC}}(\theta) = \frac{\varepsilon_0 N_f}{G_s}\left(L_f^2 - L_{\mathrm{fo}}^2\right) > 0. \quad (8)$$

Since $\mathrm{PI}_{\mathrm{SVC}}(\theta)$ is always positive, there is no pull-in. We will show later that this conclusion is not valid when we consider

$$C_{\mathrm{AVC}}(\theta) = \begin{cases} \dfrac{\varepsilon_0 N_f}{G_s(\theta_i - \theta)}\left\{T_f - L_{\mathrm{fo}}(\theta_i - \theta)\right\}^2, & \text{if } 0 \leq \theta \leq \theta_i - \dfrac{T_f}{L_f} = \theta_C \quad (2\mathrm{a}) \\[4mm] \dfrac{2\varepsilon_0 N_f}{G_s}\left\{T_f(L_f - L_{\mathrm{fo}}) - \dfrac{\left(L_f^2 - L_{\mathrm{fo}}^2\right)}{2}(\theta_i - \theta)\right\}, & \text{if } \theta_C < \theta \leq \theta_i \quad (2\mathrm{b}) \end{cases}$$

$$\mathrm{PI}_{\mathrm{AVC}}(\theta) = \begin{cases} \dfrac{\varepsilon_0 N_f}{G_s}\dfrac{T_f^2(\theta_i - 3\theta) - L_{\mathrm{fo}}^2(\theta_i - \theta)^3}{(\theta_i - \theta)^3}, & \text{if } 0 \leq \theta \leq \theta_C \quad (3\mathrm{a}) \\[4mm] \dfrac{\varepsilon_0 N_f}{G_s}\left(L_f^2 - L_{\mathrm{fo}}^2\right) > 0, & \text{if } \theta_C < \theta \leq \theta_i \quad (3\mathrm{b}) \end{cases}$$
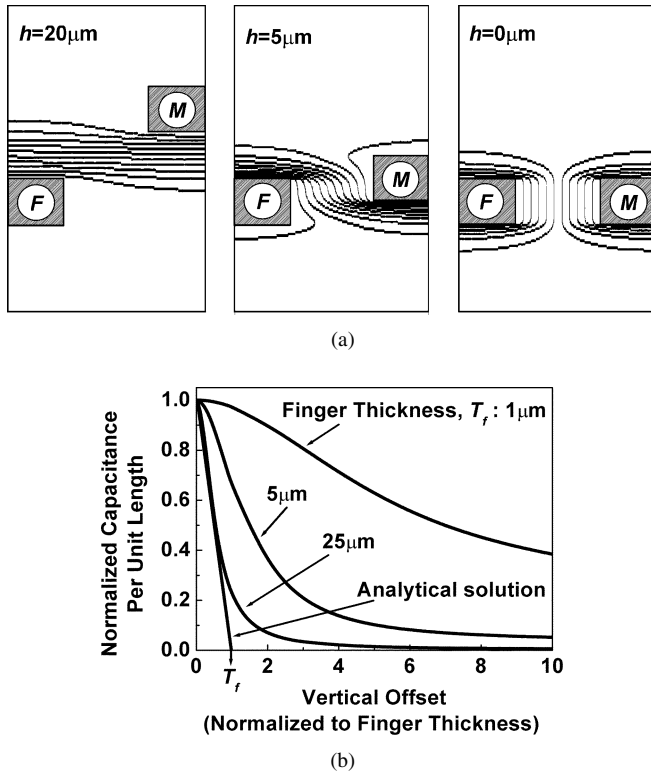
(a)

(b)

Fig. 3. (a) Electric potential distribution of the unit cell of the comb for various vertical offset between the moving and the fixed fingers (h). (b) Calculated normalized capacitance ($C_{\text{unit}}(h)/C_{\text{unit}}(0)$) as a function of the normalized vertical offset (h/T_f) for various finger thicknesses (T_f). In (a) and (b), lateral finger spacing (G_s) and finger width (W_f) are 3 and 5 μm, respectively.

nonzero H_{offset}. The maximum continuous rotation angle of SVC ($\theta_{M,\text{SVC}}$) is determined as the angle ($\theta_{\text{mc, SVC}}$) at which $C_{\text{SVC}}(\theta)$ reaches maximum

$$\theta_{M,\text{SVC}} = \frac{T_f}{L_f}. \qquad (9)$$

Comparing (6) and (9), the AVC has 50% larger continuous scan range than the SVC for the same finger geometries.

B. Hybrid Model

In this section, we present a hybrid model that combines 2-D finite-element analyses with analytic formulations. This hybrid model takes into account the fringe field and allows us to calculate precisely the pull-in conditions and pull-in angles for various geometries. Compare with the full 3-D finite-element analysis, the hybrid model is much faster and can be used for device design and parametric analysis. The simulation procedure is summarized in the following.

First the 2-D capacitance of a unit cell in the cross section of the comb is calculated for various offset (h) between the moving and the fixed finger [Fig. 3(a)]. The unit cell consists of half of a moving finger and half of a fixed finger with periodic boundary condition. We used MATLAB to calculate the electrical potential distribution (P) for a given bias voltage V and then find the electric charges (ρ) on the electrode using Poisson's equation ($\nabla^2 P = -(\rho/\varepsilon_0)$). The unit capacitance is obtained by integrating the charges over the periphery of the finger $C_{\text{unit}}(h) = (\int \rho)/V$. Fig. 3(b) shows the normalized unit capacitance versus the finger offset for three different

finger thicknesses. The finger offset h is normalized to the finger thickness T_f. The effect of fringe field is evident by the nonzero capacitance when the offset is larger than the finger thickness i.e., $h/T_f > 1$. The parallel-plate approximation is shown by the straight line. For thick fingers (25 μm), the exact capacitance follows the parallel-plate approximation reasonably well at small offset. However, when the offset is close to the finger thickness, the fringe fields dominate and exact capacitance deviates from the straight line. For small finger thickness (e.g., 1 μm), the fringe field is nonnegligible even for a small offset, and the exact solution is far from the parallel-plate approximation.

The total capacitance as a function of rotation angle for the AVC and the SVC are calculated by the following expression:

$$C_{\text{AVC}}(\theta) = 2N_f \int_{L_{\text{fo}}}^{L_f} C_{\text{unit}}(h_{\text{AVC}}(\theta,l)) \, dl \qquad (10)$$

$$C_{\text{SVC}}(\theta) = 2N_f \int_{L_{\text{fo}}}^{L_f} C_{\text{unit}}(h_{\text{SVC}}(\theta,l)) \, dl \qquad (11)$$

where $h_{\text{AVC}}(\theta,l) = l\sin(\theta_i - \theta)$ and $h_{\text{SVC}}(\theta,l) = T_f + H_{\text{offset}} - l\sin(\theta)$. Once the capacitance function is found, we can use (1) in order to determine whether pull-in phenomena exist and in order to calculate the pull-in angle. To simplify the calculation, the unit capacitance as a function of finger offset is fitted analytically, and the remaining part of the calculation can be performed analytically. It should be pointed out that the 2D finite-element calculation of the capacitance only needs to be performed once for a given finger thickness and gap spacing. Design variations involving different finger lengths, initial comb angles, and vertical and longitudinal offset of comb fingers can be obtained analytically. The model described here does not include the end effects at the finger tips. The tip effect is negligible for finger length much larger than the gap spacing, which is true for most practical actuators.

Fig. 4(a) shows the calculated pull-in investigation function, PI(θ) for AVC for three different initial comb angles: $\theta_i = 6°$, 8.2°, and 10°. The finger gap spacing, width, thickness, length, and offset length are set to be 3, 5, 10, 200, and 5 μm, respectively. For small initial comb angle ($\theta_i = 6°$), PI(θ) is always positive, indicating the AVC is stable throughout the entire angle. The maximum continuous rotation angle is equal to the initial comb angle for that case. For larger initial comb angle ($\theta_i = 8.2°$), PI(θ) intersects tangentially with the horizontal axis. The AVC is on the verge of pull-in. For even larger initial comb angle ($\theta_i = 10°$), the AVC exhibits pull-in. PI(θ) intersects with the horizontal axis twice. The smaller intersection angle is the pull-in angle of the AVC. The larger intersection angle is not meaningful. Similarly, the pull-in investigation function for the SVC can also be plotted for varying vertical offset between the moving and the fixed combs H_{offset} [Fig. 4(b)]. Two similar regimes of operation can be identified also: continuous operation for small H_{offset} and bistable operation with pull-in for large H_{offset}.

For scanning mirror applications, we are interested in the maximum continuous rotation angle (θ_M). Fig. 4(c) plots θ_M of the AVC and the SVC as functions of the initial comb angle and the vertical offset, respectively. Two regimes of operation
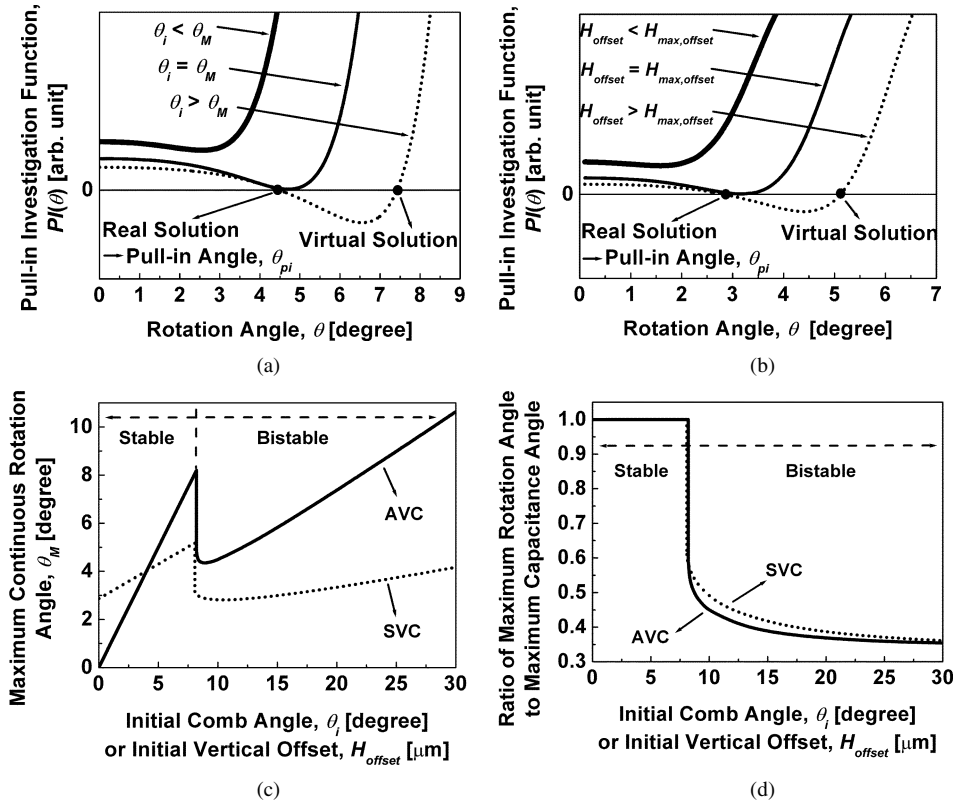
Fig. 4. (a) Calculated pull-in investigation function [PI(θ)] when initial comb angle ($\theta_i = 6°$) < maximum scan angle ($\theta_M = 8.2°$) (thick solid line), $\theta_i = \theta_M$ (thin solid line), and $\theta_i(10°) > \theta_M$ (dotted line) of the AVC. (b) Calculated PI(θ) when initial vertical offset ($H_{\text{offset}} = 3\,\mu$m) < maximum allowable vertical offset without pull-in ($H_{\text{max,offset}} = 8.1\,\mu$m) (thick solid line), $H_{\text{offset}} = H_{\text{max,offset}}$ (thin solid line), and $H_{\text{offset}}(12\,\mu$m) > $H_{\text{max,offset}}$ (dotted line) of the SVC. (c) Calculated maximum continuous rotation angle (θ_M) as a function of θ_i (AVC) or H_{offset} (SVC). (d) Calculated ratio of θ_M to maximum capacitance angle (θ_{mc}) as a function of θ_i or H_{offset}. In (a)–(d), lateral finger spacing (G_s), finger width (W_f), finger thickness (T_f), finger length (L_f), and finger offset length (L_{fo}) are 3, 5, 10, 200, and 5 μm, respectively, and the hybrid model is used.

can be clearly identified. For small initial comb angles (left part of the solid curve), the AVC is stable for all rotation angles. The maximum rotation angle is equal to the initial comb angle. For large initial comb angles (right part of the solid curve), the AVC becomes bistable and the maximum angle is equal to the pull-in angle. The vertical offset plays a similar role for the SVC as the initial comb angle for AVC, as shown by the dotted curve in Fig. 4(c). In Fig. 4(d), we plot the ratio of the maximum continuous rotation angle and the maximum-capacitance angle (θ_{mc}) as functions of the initial come angle and the vertical offset for the AVC and the SVC, respectively. In the stable regime, the ratio is exactly one. As the actuators enter the bistable regimes, the ratio reduced abruptly. As the initial comb angle (or the vertical offset) increases to large values, the ratio approaches 1/3, mimicking that of the classical parallel-plate electrostatic actuators.

For most beamsteering applications, it is desirable to design the actuators in the pull-in-free regime. Large continuous scan range can be obtained. In Section II-C, we will focus on the parametric analysis of the maximum continuous scan angle in the stable regime for both AVC and SVC. We will also compare the performance of these two actuators for the same comb finger dimensions.

C. Parametric Analysis of Maximum Continuous Rotation Angles

For the pull-in-free design, the maximum continuous scan range θ_M is equal to the maximum-capacitance angle, which

is θ_i for the AVC and $\sin^{-1}((T_f + H_{\text{offset}})/L_f)$ for the SVC. The θ_M for the AVC is found by gradually increasing θ_i until (1) has a solution. Similarly, the θ_M for SVC is found by gradually increasing H_{offset} until (1) equals zero. Fig. 5(a) shows the maximum rotation angle versus the finger thickness for the AVC (solid line) and the SVC (dotted line). The results of both hybrid and analytical models are shown for comparison. There are several interesting trends. First, the θ_M increases with finger thickness for both the AVC and the SVC. Increasing finger thickness is the most effective way to increase the rotation angle. Second, the analytic model underestimates θ_M. When the fringe field is not considered, the capacitance versus angle becomes steeper than the actual function. Mathematically, this hastens the occurrence of pull-in and reduces θ_M. The underestimation is more pronounced at small finger thickness, where the contribution of the fringe capacitance is more important, as shown in Fig. 3(b). Third, as predicted in the analytic model, the AVC has larger θ_M than the SVC, though the ratio of the maximum angles is not exactly 1.5. We will discuss the ratio in more detail later.

The effect of finger thickness on the onset of pull-in is somewhat different for the AVC and the SVC. The AVC with thicker fingers allows larger θ_i before pull-in can occur, as shown by the solid curve in Fig. 5(a). On the other hand, the SVC with thicker fingers permits less vertical offset between the moving and the fixed combs to avoid pull-in. Fig. 5(b) shows the maximum allowable vertical offset without pull-in
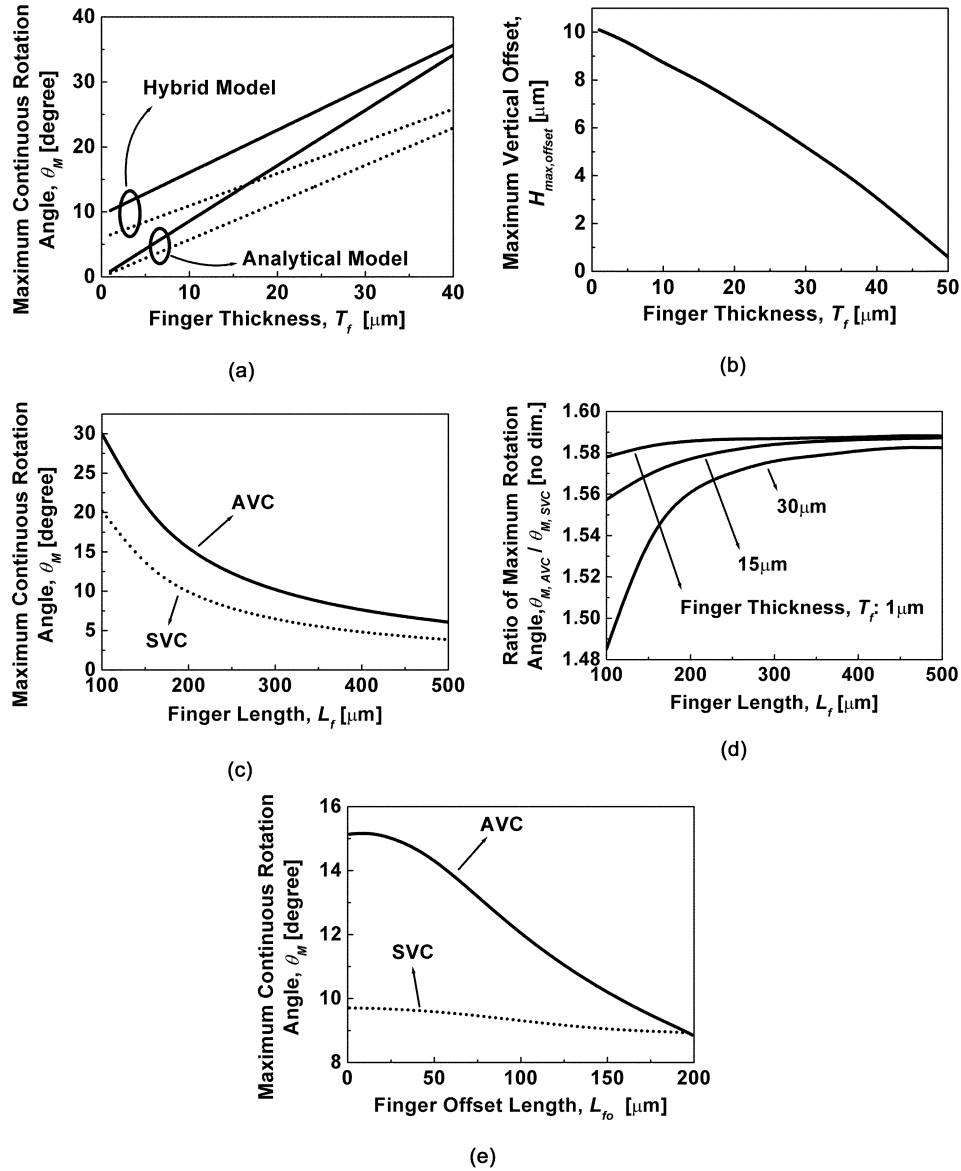
Fig. 5. (a) Calculated maximum continuous rotation angle without pull-in (θ_M) of AVC (solid line) and SVC (dotted line) as a function of finger thickness (T_f) by using the hybrid model and the analytical model (finger length (L_f): 100 μm and finger offset length ($L_{\rm fo}$): 5 μm). (b) Calculated maximum vertical offset without pull-in ($H_{\rm max,offset}$) as a function of T_f in SVC (L_f: 100 μm and $L_{\rm fo}$: 5 μm). (c) Calculated θ_M as a function of L_f (T_f: 30 μm and $L_{\rm fo}$: 5 μm). (d) Calculated ratio of θ_M of AVC to that of SVC as a function of L_f for various T_f ($L_{\rm fo}$: 5 μm). (e) Calculated θ_M as a function of $L_{\rm fo}$ (T_f: 30 μm and L_f: 200 μm). In all cases, lateral finger spacing (G_s) and finger width (W_f) are 3 and 5 μm, respectively. The results in (b)–(e) are generated by using the hybrid model.

($H_{\rm max,offset}$) versus the finger thickness. It decreases monotonically from 10 μm at $T_f = 1$ μm to 3 μm at $T_f = 40$ μm.

The effect of finger length on θ_M is shown in Fig. 5(c). The finger thickness and offset length are fixed at 30 and 5 μm, respectively. The maximum rotation angles for both the AVC and the SVC reduce as the finger lengths increases, primarily because the geometric angle (T_f/L_f) spanned by the finger thickness reduces. Larger maximum angles can be achieved with shorter fingers, at the expense of higher voltage. For all finger lengths, the AVC has higher θ_M than the SVC. Fig. 5(d) shows the ratio of the maximum continuous angles for the AVC and the SVC ($\theta_{M,\rm AVC}/\theta_{M,\rm SVC}$) versus the finger lengths for three different finger thicknesses: 1, 15, and 30 μm. The ratio approaches 1.6 for long finger lengths. This is larger than the ratio

predicted by the analytic model (1.5) due to the contributions of the fringe field. The ratio reduces slightly for thicker fingers because of less contribution of fringe capacitance. The effect of finger offset on θ_M is shown in Fig. 5(e). It has little effect on the SVC. On the other hand, it is important to keep the finger offset as small as possible for the AVC to maintain large initial capacitance.

D. Other Design Considerations for AVC

In our analysis so far, we have assumed the axis of the AVC ($A_{\rm AVC}$) is aligned with the mechanical rotation axis (A_M) defined by torsion springs. In the most straightforward layout, the axis of the AVC is often offset from the rotation axis, as shown
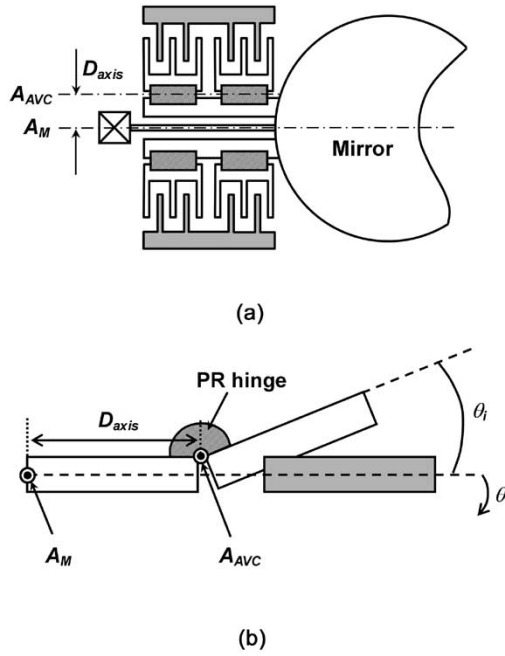
(a)

(b)

Fig. 6. Schematic diagrams of the AVC when the axis of AVC (A_{AVC}) is offset from the mechanical rotation axis (A_M) defined by the torsion bars. (a) Top view. (b) Cross-section view.
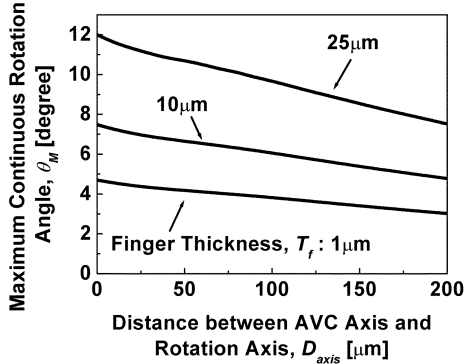

Fig. 7. Calculated maximum continuous rotation angle (θ_M) as a function of distance between AVC axis (A_{AVC}) and mechanical rotation axis (A_M), D_{axis} for various finger thicknesses (T_f) in AVC. The hybrid model is used. (Lateral gap spacing (G_s): 3 μm, finger width (W_f): 5 μm, finger length (L_f): 200 μm, and finger offset length (L_{fo}): 60 μm).

in Fig. 6. In this case, total capacitance (C'_{AVC}) is calculated according to

$$C'_{\mathrm{AVC}}(\theta) = 2N_f \int_{L_{\mathrm{fo}}}^{L_f} C_{\mathrm{unit}}\left(h'_{\mathrm{AVC}}(\theta, l)\right) dl \qquad (12)$$

where $h'_{\mathrm{AVC}}(\theta, l) = l\sin(\theta_i - \theta) - D_{\mathrm{axis}}\sin(\theta)$ and D_{axis} is the distance between the two axes. Fig. 7 shows calculated maximum continuous rotation angle versus the offset of the AVC axis. In the presence of offset, the maximum-capacitance angle is no longer equal to the initial comb angle. As a result, θ_M reduces gradually with increasing offset. The reduction is more pronounced for thick fingers. Therefore, it is important to minimize the offset of AVC axis in the design. For a unidirectional actuator, the AVC axis can be aligned with the rotation axis by employing an offset torsion spring, as shown in Fig. 8(a). Bidirectional actuators with aligned AVC axes can be achieved
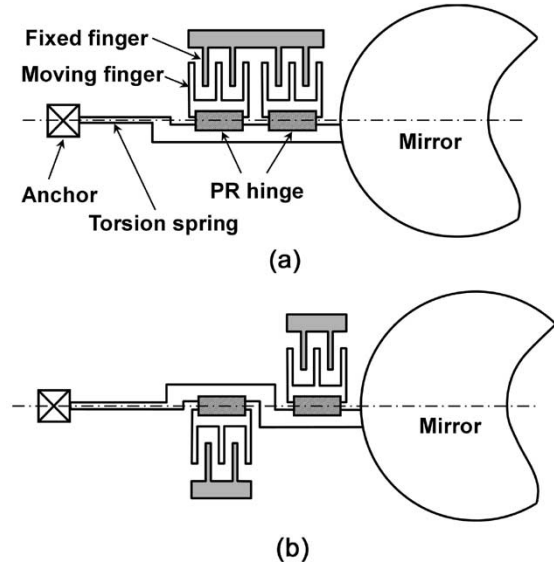

(a)

(b)

Fig. 8. (a) Schematic diagram of a unidirectional AVC (the AVC axis, A_{AVC} is same as the mechanical rotation axis, A_M). (b) Schematic diagram of a bidirectional AVC where A_{AVC} is same as A_M.
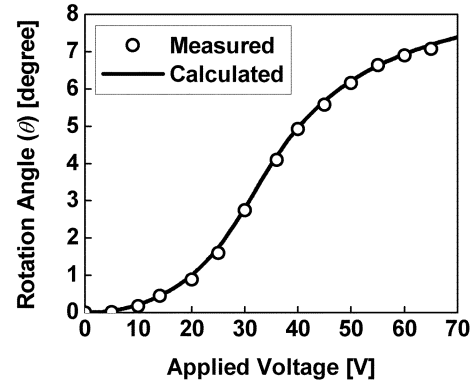

Fig. 9. The measured (symbol) and the calculated (line, hybrid model) dc scanning characteristics of AVC of which geometric parameters are summarized in Table I.

by separating the two AVCs for up and down rotations, as shown in Fig. 8(b). This, however, increases the total length and area of the scanner.

III. EXPERIMENTAL RESULTS

Fig. 9 shows the measured and the calculated (hybrid model) dc scanning characteristics of a fabricated AVC micromirror with the dimensions shown in Table I [17]. The initial comb angle (BCB hinge) was measured to be 12.4° by using the optical interferometric profiler WYKO. Excellent agreement between the experimental measurement and the calculated data was achieved. This demonstrates the effectiveness of the hybrid model. The maximum continuous rotation angle is calculated to be 8.8°, which is smaller than initial comb angle due to the nonzero offset of the AVC axis (50 μm). If θ_i is increased to 20°, θ_M can go up to 14.2° even with such an offset. Practically, the actuator is rotated continuously up to 7.2° at 65 V, and then the moving fingers are pulled-in in the y direction [see Fig. 2(a)] when the voltage is increased further. Pull-in in that direction

was not considered in the calculation. Simulation of pull-in considering secondary degree of freedom can be performed by employing more complicated numerical analysis [18]. The design can be further optimized to extend θ_M by increasing distance between the tip and the base of the fingers, increasing θ_i, and/or reducing D_{axis}. The measured resonant frequency for rotation was 598 Hz.

IV. CONCLUSION

A hybrid model has been developed for parametric analysis of the AVC and the SVC scanning micromirrors. The hybrid model includes the effect of fringe field through the 2-D finite-element calculation of the capacitance between finger electrodes. The maximum continuous scan angles are solved analytically. Our results show that the scan angle of the AVC is up to 60% larger than that of the SVC for the same finger geometries. Parametric variations for increasing the maximum scan angles are described, including thicker and shorter fingers, larger initial comb angles (larger offset for the SVC), and aligning the AVC axis with the mechanical rotation axis. The calculated results are compared with an AVC scanner fabricated on an SOI substrate with a 1-mm-diameter mirror. Excellent agreement between the experimental data and the hybrid 2-D model is obtained.

ACKNOWLEDGMENT

REFERENCES

[1] R. Conant, J. Nee, K. Lau, and R. S. Muller, "A flat high-frequency scanning micromirror," in *Tech. Dig. 2000 Solid-State Sensor and Actuator Workshop*, pp. 6–9.
[2] J.-H. Lee, Y.-C. Ko, D.-H. Kong, J.-M. Kim, K. B. Lee, and D.-Y. Jeon, "Fabrication of silicon optical scanner for laser display," in *Proc. IEEE/LEOS Int. Conf. Optical MEMS*, 2000, pp. 13–14.
[3] U. Krishnamoorthy, D. Lee, and O. Solgaard, "Self-aligned vertical electrostatic combdrives for micromirror actuation," *J. Microelectromech. Syst.*, vol. 12, pp. 458–464, Aug. 2003.
[4] J.-L. A. Yeh, H. Jiang, and N. C. Tien, "Integrated polysilicon and DRIE bulk silicon micromachining for an electrostatic torsional actuator," *J. Microelectromech. Syst.*, vol. 8, pp. 456–465, Dec. 1999.
[5] O. Tsuboi, Y. Mizuno, N. Koma, H. Soneda, H. Okuda, S. Ueda, I. Sawaki, and F. Yamagishi, "A rotational comb-driven micromirror with a large deflection angle and low drive voltage," in *Proc. IEEE Micro Electro Mechanical Systems (MEMS '02)*, pp. 532–535.
[6] V. Milanovic, S. Kwon, and L. P. Lee, "Monolithic vertical combdrive actuators for adaptive optics," in *Proc. IEEE/LEOS Int. Conf. Optical MEMS*, 2002, pp. 57–58.
[7] J. Hsieh, C. C. Chu, J. M. L. Tsai, and W. Fang, "Using extended BELST process in fabricating vertical comb actuator for optical application," in *Proc. IEEE/LEOS Int. Conf. Optical MEMS*, 2002, pp. 133–134.
[8] D. Hah, S. T.-Y. Huang, J.-C. Tsai, H. Toshiyoshi, and M. C. Wu, "Low-voltage, large-scan angle MEMS analog micromirror arrays with hidden vertical comb-drive actuators," *J. Microelectromech. Syst.*, vol. 13, pp. 279–289, Apr. 2002.
[9] P. R. Patterson, D. Hah, H. Chang, H. Toshiyoshi, and M. C. Wu, "An angular vertical comb drive actuator for scanning micromirrors," in *Proc. Int. Conf. Optical MEMS*, 2001, pp. 25–26.
[10] P. R. Patterson, D. Hah, H. Nguyen, H. Toshiyoshi, R.-M. Chao, and M. C. Wu, "A scanning micromirror with angular comb drive actuation," in *Proc. IEEE Micro Electro Mechanical Systems (MEMS '02)*, pp. 544–547.
[11] H. Xie, Y. Pan, and G. K. Fedder, "A CMOS-MEMS mirror with curled-hinge combdrives," *J. Microelectromech. Syst.*, vol. 12, pp. 450–457, Aug. 2003.
[12] J. Kim, H. Choo, L. Lin, and R. S. Muller, "Microfabricated torsional actuator using self-aligned plastic deformation," in *Proc. Int. Conf. Solid State Sensors, Actuators and Microsystems (Transducers '03)*, pp. 1015–1018.
[13] W. Piyawattanametha, P. R. Patterson, D. Hah, H. Toshiyoshi, and M. C. Wu, "A surface and bulk micromachined angular vertical combdrive for scanning micromirrors," presented at the Tech. Dig. Optical Fiber Communication Conf. (OFC 2003), Paper TuN1.
[14] H. D. Nguyen, D. Hah, P. R. Patterson, R. Chao, W. Piyawattanametha, E. K. Lau, and M. C. Wu, "Angular vertical comb-driven tunable capacitor with high-tuning capabilities," *J. Microelectromech. Syst.*, vol. 13, pp. 406–413, Jun. 2004.
[15] A. Selvakumar and K. Najafi, "Vertical comb array microactuators," *J. Microelectromech. Syst.*, vol. 12, pp. 440–449, Aug. 2003.
[16] D. Hah, H. Toshiyoshi, and M. C. Wu, "Design of electrostatic actuators for MOEMS," in *Proc. Symp. Design, Test, Integration and Packaging of MEMS/MOEMS (DTIP2002)*, pp. 200–207.
[17] P. R. Patterson, "MEMS scanning micromirrors with a new electrostatic angular vertical combdrive," Ph.D. dissertation, Univ. California, Los Angeles, 2003.
[18] D. Elata, O. Bochobza-Degani, S. Feldman, and Y. Nemirovsky, "Secondary DOF and their effect on the instability of electrostatic MEMS devices," in *Proc. IEEE Micro Electro Mechanical Systems (MEMS '03)*, pp. 177–180.

Dooyoung Hah received the M.S. and the Ph.D. degrees in electrical engineering from the Korea Advanced Institute of Science and Technology (KAIST) in 1996 and 2000, respectively. His Ph.D. thesis topic was the RF microelectromechanical (MEM) switch.

From 2000 to 2001, he was a Postdoctoral Research Engineer at the University of California, Los Angeles. From 2002 to 2004, he was a Senior Member of Research Staff at the Electronics and Telecommunications Research Institute (ETRI). He is currently a Staff Research Associate at the University of California, Los Angeles. His research interests include optical microelectromechanical systems (MOEMS), RF MEMS, and microactuators.

Dr. Hah was the third-place winner at the student paper competition at the 2000 IEEE Microwave Theory and Techniques Society (MTT-S) International Microwave Symposium.

Pamela R. Patterson (S'98–M'03) received the B.S. degree (*cum laude*) from the University of Cincinnati, Cincinnati, OH, in 1978 and the M.S. and Ph.D. degrees in electrical engineering from the University of California, Los Angeles (UCLA), in 1985 and 2003, respectively, completing the dissertation year as a recipient of an Intel Foundation fellowship.

She has held Senior Engineering positions at TRW, Varian, and UCLA, where she helped to establish the Nanoelectronics Research Laboratory from 1994 to 2003. In 2003, she joined HRL Laboratories, LLC, Malibu, CA, as a Research Staff Member and is currently conducting research on heterogeneous integration of semiconductor materials. She has authored or coauthored 14 conference papers, including three invited papers, and contributed a book chapter (coauthored with Dr. M. Wu) in the field of optical MEMS devices. Her research interests are in the area of microfabrication/nanofabrication process design and technology.

Dr. Patterson is a Member of the American Association for the Advancement of Science (AAAS), the American Vacuum Society (AVS), and Eta Kappa Nu.

Hung D. Nguyen (S'98) received the B.S. degree in physics and the M.S. degree in electrical engineering from the University of California, Los Angeles (UCLA), in 1998 and 2003, respectively. He is currently working toward the Ph.D. degree in electrical engineering at UCLA.

His research interests are mainly in optical microelectromechanical systems (MOEMS) and RF MEMS.

Mr. Nguyen is a recipient of the Intel Foundation Fellowship for 2004.

Hiroshi Toshiyoshi (M'97) received the M.Eng. and Ph.D. degrees in electrical engineering from the University of Tokyo, Tokyo, Japan, in 1993 and 1996, respectively.

From 1996 to 2001, he was a Ph.D. Lecturer with the Institute of Industrial Science (IIS), University of Tokyo. From 1999 to 2001, he was a Visiting Assistant Professor at University of California, Los Angeles, for his sabbatical years. Since 2001, he has been with the IIS as a Co-Director of the Laboratory for Integrated MicroMechatronic Systems (LIMMS), a joint research group between IIS and Centre National de la Recherche Scientifique (CNRS), France. Since 2002, he has also been an Assistant Professor of VLSI Design and Education Center (VDEC) attached to the University of Tokyo. His research interest is MEMS for free-space optics and nanomechatronics.

Ming C. Wu (S'82–M'83–SM'00–F'02) received the B.S. degree in electrical engineering from National Taiwan University in 1983, and the M.S. and Ph.D. degrees in electrical engineering and computer sciences from the University of California, Berkeley, in 1985 and 1988, respectively.

From 1988 to 1992, he was a Member of Technical Staff at AT&T Bell Laboratories, Murray Hill, NJ. In 1993, he joined the faculty of the Electrical Engineering Department, University of California, Los Angeles (UCLA), where he is currently a Professor. He is also Director of UCLA's Nanoelectronics Research Facility and Vice Chair for Industrial Relations. He has published over 340 papers, contributed four book chapters, and holds 11 U.S. patents. His current research interests include microelectromechanical systems (MEMS), optical MEMS (MOEMS), biophotonics, microwave photonics, and high-speed optoelectronics.

Dr. Wu was the Founding Cochair for the IEEE Laser and Electro-Optics Society (LEOS) Summer Topical Meeting on Optical MEMS in 1996. The meeting has now evolved into the IEEE LEOS International Conference on Optical MEMS, hosted in Europe, Asia, and the United States. He has also served in program committees of many other conferences, including Optical Fiber Communications (OFC), the Conference on Lasers and Electrooptics (CLEO), the IEEE Conference on Micro Electro Mechanical Systems (MEMS), the LEOS Annual Meetings (LEOS), the International Electron Device Meeting (IEDM), the Device Research Conference (DRC), the International Solid-State Circuit Conference (ISSCC), and Microwave Photonics (MWP). He is a David and Lucile Packard Foundation Fellow (1992–1997).